



## 3D structure of the Gusev Crater region

Mirjam van Kan Parker<sup>a,\*</sup>, Tanja Zegers<sup>b</sup>, Thomas Kneissl<sup>c</sup>, Boris Ivanov<sup>d</sup>,  
Bernard Foing<sup>e</sup>, Gerhard Neukum<sup>c</sup>

<sup>a</sup> Faculty of Earth and Life Sciences, VU University Amsterdam, De Boelelaan 1085, 1081 HV Amsterdam, The Netherlands

<sup>b</sup> Faculty of Geosciences, Utrecht University, Budapestlaan 4, 3508 TA, Utrecht, The Netherlands

<sup>c</sup> Institute of Geosciences, Planetology and Remote Sensing, Freie Universität Berlin, Malteserstrasse 74-100, Bldg D, 12249 Berlin, Germany

<sup>d</sup> Institute for Dynamics of Geospheres, Russian Academy of Sciences, Leninsky Prospekt 38, Moscow 119334, Russia

<sup>e</sup> European Space Agency (ESA), European Space & Technology Centre (ESTEC), P.O.Box 299, 2200 AG Noordwijk, The Netherlands

### ARTICLE INFO

#### Article history:

Accepted 7 January 2010

Available online 29 January 2010

#### Keywords:

Mars  
Gusev Crater  
structural geology  
stratigraphy  
Columbia Hills  
crater count ages

### ABSTRACT

Gusev Crater lies within the Aeolis Quadrangle of Mars at the boundary between the northern lowlands and southern highlands. The ancient valley Ma'adim Vallis dissects the highlands south of Gusev Crater and is thought to have fed the crater with sediments.

High Resolution Stereo Camera data and Digital Elevation Models were used to construct a geologic–geomorphic map (173.5–178.5° E, 10–18° S) and cross-sections, complemented by data from Mars Orbiter Camera, Mars Orbiter Laser Altimeter and Thermal Emission Imaging System.

Three geologic domains are recognised: the highlands in the south, Gusev Crater and lowlands in the north. Twelve units are mapped, with thicknesses ranging from hundred meters to several kilometres. Thicknesses of units, and their bedding attitude, are estimated combining the geologic map and topographic information. Relative ages are determined from crater counts, ranging from Early Noachian for highland units to Middle Amazonian for units in Gusev Crater and in lowlands. Episodes of intense geologic activity (deposition, volcanism, deformation) occur at around 4.0 Ga, 3.7 Ga, and 3.5 Ga. Comparing the geometry of the Gusev Crater with similar sized, filled and un-filled, Martian craters, suggests that the Columbia Hills are relics of the original central peak of Gusev Crater.

© 2010 Elsevier B.V. All rights reserved.

## 1. Introduction

Unravelling the geologic evolution of a planetary region requires integration of high quality satellite data, ideally combined with in-situ analytical data and observations from a lander or rover. Understanding the wider geological context of an area is essential to analyse lander or rover data. Traditionally, geological and morphological analyses are primarily based on images complemented with topographic data (Scott et al., 1978; Greeley and Guest, 1987). The present study focuses on integrating geological analyses in three dimensions using primarily High Resolution Stereo Camera (HRSC) data, in order to understand stratigraphic and structural relations. The aim of this paper is to construct the genetic origin of the Columbia Hills, the Gusev Crater floor, (sub) surface and immediate surroundings.

Gusev Crater was the landing site for the Mars Exploration Rover (MER) Spirit, in January 2004 and provided critical ground observation

data (e.g. Squyres et al., 2004, 2006; McSween et al., 2004, 2006a,b; McCoy et al., 2008). Moreover, Gusev Crater region provides a section through an important part of the Martian upper crust. It is situated close to the north–south dichotomy and may have served as a sedimentary basin for Ma'adim Vallis (e.g. Schneeberger, 1989; Grin and Cabrol, 1997; Kuzmin et al., 2000; Irwin et al., 2002), a valley dissecting the highlands south of the crater. Gusev Crater region provides a record of the geologic history from early Noachian to present, with records of impacts, volcanics, fluvial-, hydrothermal and tectonic activity.

Our study of the Gusev Crater region (173.5–178.5° E and 10–18° S; Fig. 1), is based on HRSC data from Mars Express, complemented by data from Mars Orbiter Camera (MOC), Mars Orbiter Laser Altimeter (MOLA), Thermal Emission Imaging System (THEMIS), Infrared (IR) and visible. This study includes geologic mapping and derivation of cross-sections providing insight in the 3D geometry of the rock units in the region. Cross-cutting and superposition relationships are used to determine the relative sequence of geological events. Age estimates from crater counts for specific units are incorporated, providing a constraint on the geologic evolution of the area and the timing of major events. Finally a comparison with similar sized craters is used to constrain the genetic origin of the Columbia Hills.

\* Corresponding author. Tel.: +31 20 5983725; fax: +31 20 5989942.

E-mail addresses: [Mirjam.van.kan@falw.vu.nl](mailto:Mirjam.van.kan@falw.vu.nl) (M. van Kan Parker), [tanja@geo.uu.nl](mailto:tanja@geo.uu.nl) (T. Zegers), [Thomas.Kneissl@fu-berlin.de](mailto:Thomas.Kneissl@fu-berlin.de) (T. Kneissl), [baivanov@ints.ru](mailto:baivanov@ints.ru) (B. Ivanov), [Bernard.Foing@esa.int](mailto:Bernard.Foing@esa.int) (B. Foing), [gneukum@zedat.fu-berlin.de](mailto:gneukum@zedat.fu-berlin.de) (G. Neukum).

## 2. Geological context

The study area shows a variety of interesting geological features. The prime feature is the Noachian aged (Kuzmin et al., 2000) Gusev Crater itself. It has a rim to rim diameter of ~160 km centred at ~14.64° S and 175.36° E. The rim of the mostly filled crater is relatively well preserved, despite some craters superimposed on it. Previous regional studies include those by Scott et al. (1978), Greeley and Guest (1987), Grin and Cabrol (1997) and Kuzmin et al. (2000).

Other features in the area include the southern flank of the Apollinaris Patera volcano, the Medusae Fossae Formation in the northeast, the chaotic terrain in the degraded de Vaucouleurs Crater

in the west and surrounding highlands. Apollinaris Patera is an ancient shield volcano with central vent system and multiple flows, having properties consistent with basalt (Greeley and Spudis, 1981). The final stage of volcanic activity was the emplacement of deposits on its southern flank described as the more competent deposit of the volcanic construct (Robinson et al., 1993). The Medusae Fossae Formation typically occurs in equatorial regions and has been described as an extensive, geologically young and wind-scoured deposit (Scott and Tanaka, 1986; Greeley and Guest, 1987; Bradley et al., 2002; Carter et al., 2009). The Vaucouleurs chaotic terrain is part of a chain of chaotic terrains found along the dichotomy boundary (Sharp, 1973).

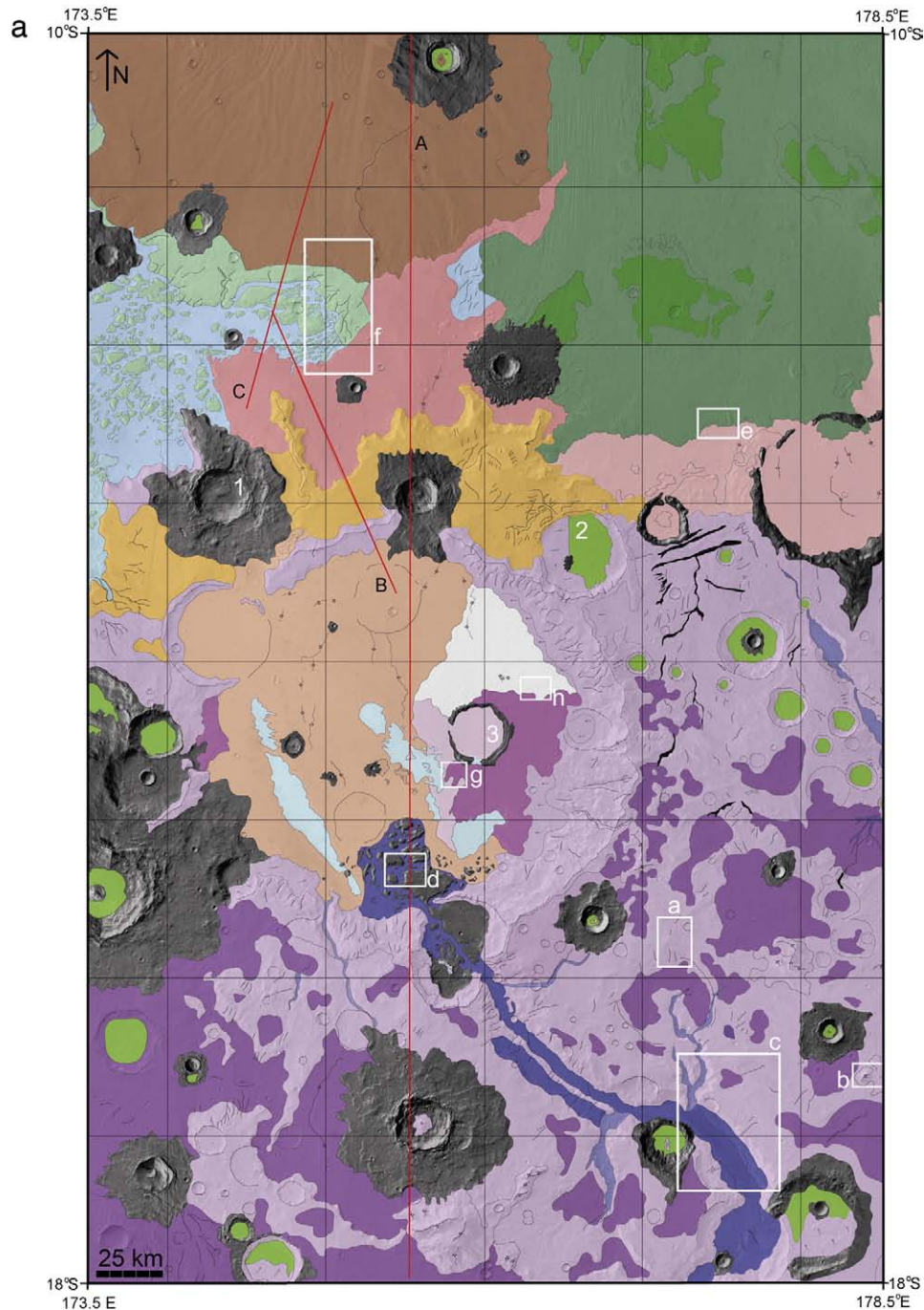


**Fig. 1.** a) Geologic map of the Gusev Crater region bounded by the coordinates 173.5–178.5° E, 10–18° S. Geologic cross-section (Fig. 2) locations are marked in black capitals. Outlined areas are the image locations for Fig. 3, a = Fig. 3a; b = 3b etc. Names of numbered craters are: 1 = Zutphen; 2 = Galdakao; 3 = Thira. b) Legend to the geological map and context image of the mapped region.

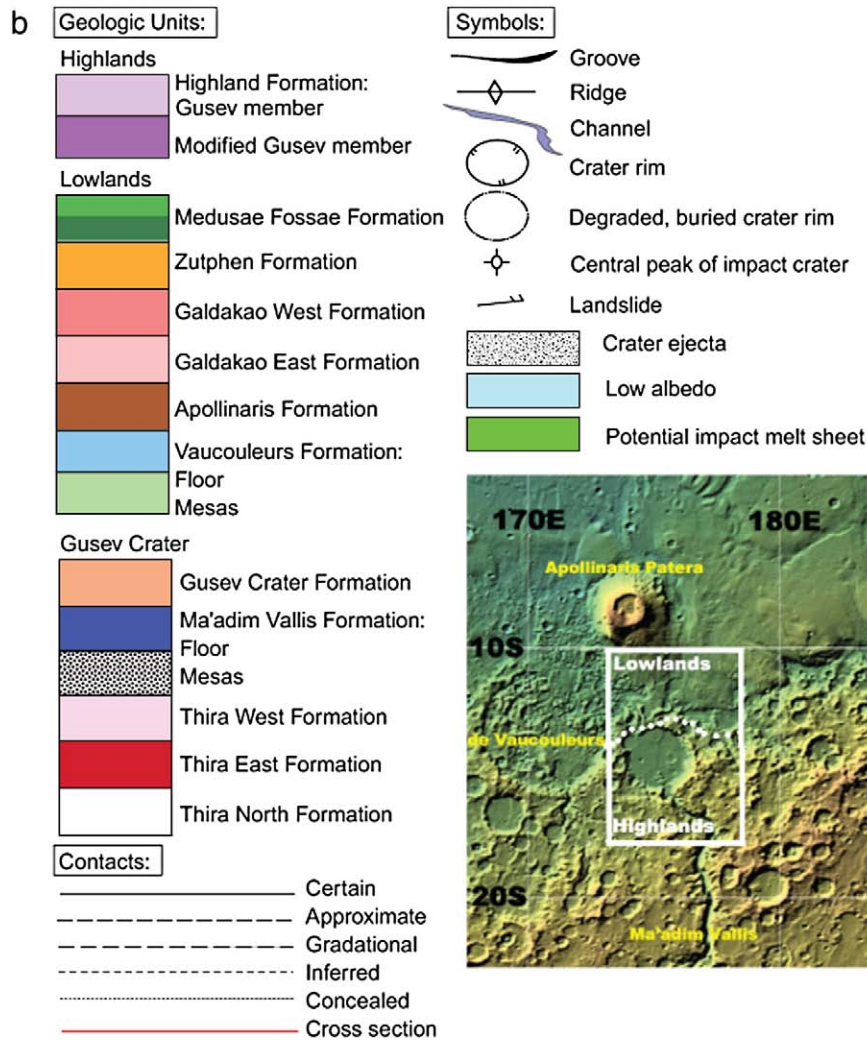


Fig. 1 (continued).

Gusev Crater is generally thought to hold clues to early fluvial activity on Mars, because Ma'adim Vallis has been interpreted as ancient fluvial system dissecting the highlands south of the crater. It is ~900 km long, has an average width of 15 km, incises Gusev Crater's southern rim and empties into the crater. Putative sediments transported by Ma'adim Vallis would have been deposited within the crater (Sharp and Malin, 1975; Schneeberger, 1989; Grin and Cabrol, 1997; Cabrol et al., 1998; Kuzmin et al., 2000; Irwin et al., 2002; Cabrol et al., 2003; Irwin et al., 2004) and a Gilbert-type delta would have formed (Kleinhaus, 2005). This sedimentary interpretation was the basis for its selection as the landing site for Mars Exploration Rover (MER) Spirit (Golombek et al., 2003). It is thought to be a prime site to provide clues to an early (wet) Mars. In anticipation of Spirit's landing Milam et al. (2003) used THEMIS and other data to characterise the deposits within the crater.

In contrast to the sedimentary interpretation, Spirit showed that the plains surrounding the landing site are composed of picritic basaltic lavas unaltered by aqueous processes (e.g. McSween et al., 2004; Golombek et al., 2006; Grant et al., 2006). Martinez-Alonso et al. (2005) and Greeley et al. (2005) showed that these basaltic plains characterising most of the crater floor postdate other crater fill materials, such as putative sediments deposited by Ma'adim Vallis.

Data returned by Spirit, as well as orbital data (Martinez-Alonso et al., 2005) have shown that the Columbia Hills are embayed by the surrounding basaltic plains. The Columbia Hills vary compositionally

from the surrounding basalts (Morris et al., 2006; Golombek et al., 2006; Squyres et al., 2006; McSween et al., 2006a,b; Wang et al., 2006a,b; Clark et al., 2007). Various rocks were analysed in Columbia Hills, including those high in phosphorous, potential pyroclastic or impact materials (so-called Wishstone class rocks; Squyres et al., 2006) and aqueously altered rocks (so-called Clovis and Washtower class rocks; Squyres et al., 2006; Clark et al., 2007). McCoy et al. (2008) used 3D imaging software to show that the dips of bedding on the main edifice of Columbia Hills are steeper than the local topography and that there is a significant variation in dip angle within Columbia Hills.

### 3. Methodology

#### 3.1. Image data and mapping

HRSC data (0.68  $\mu\text{m}$ ), stereoscopic anaglyphs and Digital Elevation Models (DEM's) were used for the geologic–geomorphic mapping and construction of geologic cross-sections. Units were mapped based on morphological and thermophysical characteristics, similar to the approach of Milam et al. (2003). Morphology and structure were derived from (stereo) image data (HRSC, THEMIS IR day, MOC) and thermophysical properties (albedo and thermal inertia) were additionally derived from HRSC and THEMIS IR image data. Inertia gives an indication to the type of material, i.e. compact rocky material, as

opposed to loose dust (Mellon et al., 2000). Thermophysical characteristics were qualitatively assessed. Albedo was defined as low (dark areas) or high (light areas). Day and night temperatures were assessed using THEMIS IR images, where dark reflects cold areas and light reflects warm regions. Unit boundaries were mapped based on unit characteristics (thermophysical and morphological properties, Table 1) and break

of slope. Break of slope mapping is a technique traditionally used in terrestrial geological mapping (Powell, 1992) and relates directly to the mechanical and erosional properties of rock units. It is only with the current availability of HRSC stereo data that this method using 3D information, in the form of anaglyphs (Appendix A) or DEMs can be used for geologic mapping on Mars. The 3D mapping method used resulted in

**Table 1**  
Summary of the units present within the mapped area.

Unit	Morphology and structures	Thermophysical properties	Thickness (m)*	Age (Ga)	Surface area used for crater count (km <sup>2</sup> )	Comparison to previous studies
<i>Lowlands</i>						
Medusae Fossae	-Undulating surface -Large elevation differences -Layering S boundary	High albedo, moderate day and cold night temperatures.	?	** > 1.13 <sup>+0.56</sup> <sub>-0.56</sub>	174	<sup>1</sup> Aml <sub>1</sub> , Aml <sub>2</sub>
Zutphen	-Narrow spaced ridges ~ NS orientated -Cut by increasing number of grooves and channels near Zutphen and Galdakao craters	High albedo, moderate day and moderate (in W) to cold (in E) night temperatures.	1500	3.52 <sup>±0.05</sup> <sub>0.08</sub>	614	<sup>1</sup> Hpld
Galdakao East	-Generally smooth surface -Buttes and knobs concentrated in the centre, attaining heights of 200 m. -Local presence of subdued ridges -Varying degree of erosion, locally etched surface	High albedo, moderate, moderate to cold day and cold night temperatures.	> 300	3.57 <sup>±0.06</sup> <sub>0.11</sub>	737	<sup>1</sup> AHgf <sub>1</sub> , Hcht
Galdakao West	-Generally smooth surface -Local presence of subdued ridges -Varying degree of erosion, locally etched surface	High albedo, moderate day and cold night temperatures.	≥ 900	3.85 <sup>±0.15</sup> <sub>0.15</sub>	1408	<sup>1</sup> AHgf <sub>1</sub> ,
Apollinaris	-Arc shaped deposit -Relatively smooth, slightly wavy -Layering within larger crater walls	High albedo, moderate day and night temperatures, increasing from E to W.	1000	3.76 <sup>±0.04</sup> <sub>0.06</sub>	4707	-
Vaucouleurs	-Presence of buttes and mesas in varying size, maximum 1 km high, increasing in size towards E, no specific orientation	High albedo, with local patch of low albedo, moderate day and night temperatures, valley floors generally cold at night.	> 700 (floor) 600 (mesas)	*** > 3.85 <sup>±0.15</sup> <sub>0.15</sub>	-	<sup>1</sup> Achp, Hcht, Hpld, AHbm <sub>1</sub>
<i>Gusev Crater</i>						
Thira East	-Etched, pitted and knobby surface	High albedo, moderate day and hot with locally moderate night temperatures.	200	2.89 <sup>±0.28</sup> <sub>0.44</sub>	737	<sup>1</sup> AHbm <sub>1</sub> <sup>2</sup> Etched <sup>3</sup> Plains materials, High thermal inertia rough
Thira North	-Small subdued ridges, 100 m wide, trending NE–SW -Locally more pronounced ridges	High albedo, moderate day and moderate–cold night temperatures.	100	3.52 <sup>±0.08</sup> <sub>0.16</sub>	644	<sup>1</sup> AHbm <sub>1</sub> <sup>2</sup> Wrinkled <sup>3</sup> Plains materials, Low thermal inertia
Thira West	-Rough terrain -Locally knobby appearance -Presence of lobate margins	High albedo, moderate day and night temperatures.	80	3.31 <sup>±0.09</sup> <sub>0.17</sub>	321	<sup>1</sup> AHgf <sub>1</sub> <sup>2</sup> Lobate <sup>3</sup> Plains materials, High thermal inertia smooth
Gusev Crater	-Generally smooth -Few prominent ridges -Craters: cold day and hot night T	High albedo, moderate day and night temperatures.	150	3.65 <sup>±0.06</sup> <sub>0.10</sub>	3241	<sup>1</sup> AHgf <sub>1</sub> , AHgf <sub>2</sub> <sup>2</sup> Plains <sup>3</sup> Plains materials
<i>Highlands</i>						
Ma'adim Vallis	-Cuts highlands S of Gusev -Streamlines upon entry in Gusev // to longitudinal axis of channel -Layered, flat topped mesas within Gusev inlet -Two main flooding levels, cut by tributary run-off channels	High albedo, with local low albedo patches, moderate day and night temperatures. Cold day and hot night temperatures at low albedo material.	> 450	3.58 <sup>±0.06</sup> <sub>0.10</sub> 3.79 <sup>±0.05</sup> <sub>0.08</sub>	377 666	<sup>1</sup> AHbm <sub>1</sub> , AHch <sub>1</sub> , AHch <sub>2</sub> , AHch <sub>3</sub> <sup>2</sup> Mesas, Ma'adim Vallis <sup>3</sup> Plains materials
Highland members:						
Modified Gusev	-Varying amount of grooves, valleys and run-off channels	High albedo, moderate day and night temperatures.	MG < 100 G > 2500	3.72 <sup>±0.05</sup> <sub>0.07</sub> 4.04 <sup>±0.06</sup> <sub>0.10</sub>	886 2581	<sup>1</sup> Npl, c <sub>1</sub> , HMpl <sub>1</sub> , HMpl <sub>2</sub> , Nm
Gusev Mountainous	-Rough, rugged, cratered terrain Mountainous areas show steep, narrow ridges		M > 2000	3.95 <sup>±0.05</sup> <sub>0.07</sub>	631	

<sup>1</sup>U.S.G.S. Equivalent Geologic Units Kuzmin et al. (2000); <sup>2</sup>Milam et al. (2003); <sup>3</sup>Martinez-Alonso et al. (2005).

\*Thicknesses are determined from geologic cross-sections, the thicknesses of units within the Gusev Crater serve as minimum thickness estimates, because of low topographic variations.

\*\*Age has not been directly determined, but is constrained via a younger unnamed crater.

\*\*\*Age has not been directly determined, but is constrained via surrounding units.

a geologic map and geologic cross-sections. The combination of the geologic map and cross-sections provides insight in the geometry of geologic units, such as thickness and thickness variations and bedding attitude. Since Gusev Crater floor is relatively flat, the 3D information of the present units is limited. Therefore these particular unit thicknesses are not well constrained.

MOLA topographic gridded data, THEMIS infrared (IR) and visible-IR-day: band 5, 9.35  $\mu\text{m}$ ; IR-night: band 9, 12.57  $\mu\text{m}$ ; visible band 3, 0.65  $\mu\text{m}$ ) data and MOC (0.70  $\mu\text{m}$ ) images supplemented the HRSC analysis. The HRSC data includes four orbits with an original resolution of 25 m (24, 72, 283 and 335), that covered the area obtained in the first year of Mars Express' operation, additionally orbit 2249 was used, with an original resolution of 25 m. The DEM's (Gwinner et al., 2005) derived from these orbits have a resolution of 100 m/pixel for orbits 24 and 72 and 200 m/pixel for orbits 283 and 335. The anaglyphs were derived from the nadir and stereo 1 images, which were superimposed to produce a stereo effect and were generated as red and green images for stereo viewing.

The mapped area was covered by HRSC at 80%, 95% for THEMIS IR images, 35% for THEMIS visible images and 5% coverage for MOC images. Geologic units were named after characteristic geographic features in the area, following standard procedures for naming stratigraphic units.

### 3.2. Age determination

HRSC image mosaics with a resolution of 25 m/pixel were used for crater count determination using the program "craterstats" (Michael and Neukum, 2010-this issue; Michael and Neukum, 2008). The crater measurements were recorded and partitioned into bins of increasing crater size. These binned data were used to produce cumulative crater size–frequency distribution plots including statistical errors (Appendix A, e.g., Neukum and Wise, 1976; Neukum, 1983). Cumulative size–frequency distributions were analysed to determine crater frequencies at specific reference diameters, 1-, 2-, 5-, 10-, and 16-km and crater model ages, following Hartmann and Neukum (2001). For more details on the crater age determination method see Neukum et al. (2010-this

issue). The model crater ages were calculated fitting the crater production function (Neukum, 1983; Hartmann and Neukum, 2001; Ivanov, 2001) to the data set and then applied to the Hartmann and Neukum chronology model (2001).

Since the chronology function (Hartmann and Neukum, 2001) used to transform the density into an age, is exponential beyond 3 Ga, it has the effect that error-bars extending into this age range are contracted by comparison with those in the younger linear range. Thus the magnitude of the positive age error is typically less than the negative error when dealing with older surfaces.

For some of the counted areas a second, resurfacing age is given. This age reflects a resurfacing process, e.g. erosion that changed the crater population by removing craters at the low-diameter edge of the distribution (Michael and Neukum, 2010-this issue; Michael and Neukum, 2008).

### 3.3. Gusev Crater morphology

Ivanov et al. (2005) and Werner et al. (2005) used MOLA data to study two craters (Lohse, and Bakhuysen, Crater 1 and 2 respectively) with similar diameters to Gusev Crater but located in different areas and with different geologic histories. We refined the comparative approach to reconstruct the "fresh Gusev" morphometry (i.e. the crater geometry prior to infill) by comparing it with a larger set of craters with diameters > 100 km. The data were acquired using JMars Java software (Gorelick et al., 2003) from Arizona State University ([http://jmars.asu.edu/wiki/index.php/Main\\_Page](http://jmars.asu.edu/wiki/index.php/Main_Page)). JMars uses the MOLA-based 128 dots-per-degree topographic map to portray crater morphology and plot topographic profiles.

## 4. Results

Below we discuss the results of the 3D geological analysis and the results of crater count statistics for selected surface areas based on the geological analysis.

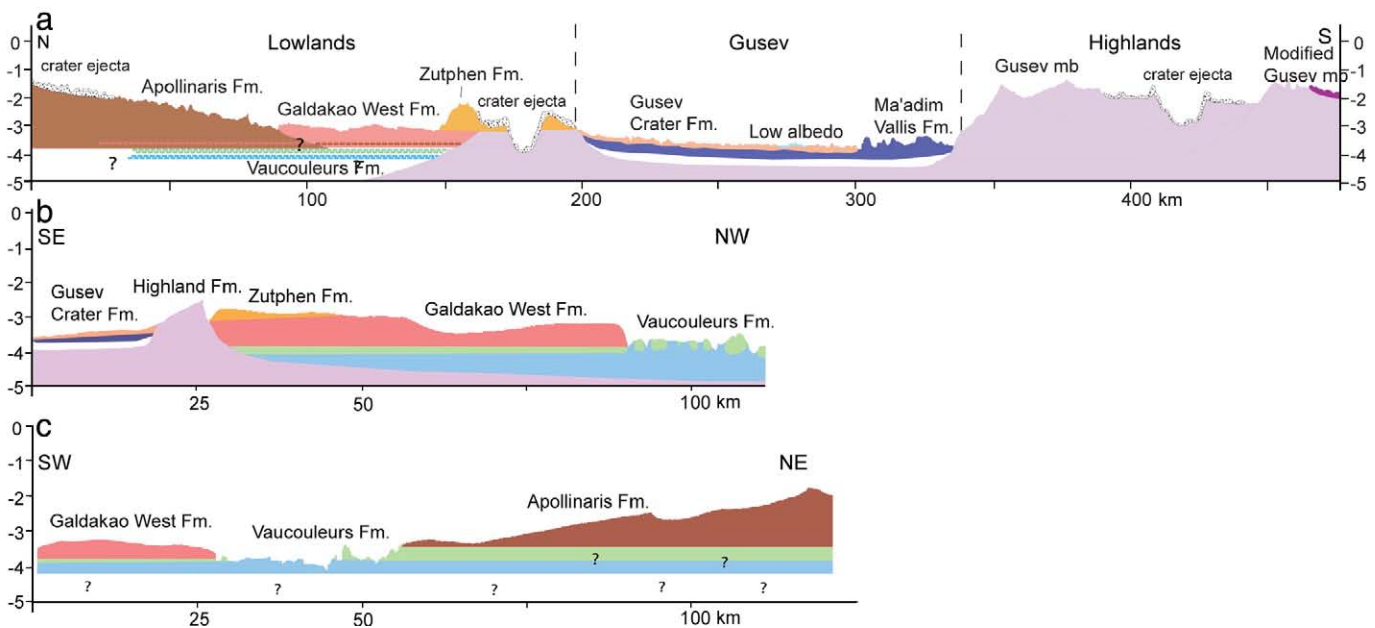


**Fig. 2.** Selected geologic cross-sections. The subsurface and stratigraphy have been interpreted from the combination of surface geology and topography. The trace of the cross-sections can be seen in the geological map in Fig. 1a. The horizontal distance and vertical elevation are in kilometres. a) North South cross-section through the mapping area. b) Cross-section through the northern rim of the Gusev Crater and the Zutphen-, Galdakao West- and Vaucouleurs-lowland formations. The relation between Galdakao West- and Vaucouleurs-Formation is also illustrated in Fig. 3f. c) Cross-section through Galdakao West-, Vaucouleurs- and Apollinaris Formation.

#### 4.1. Geologic analysis

The 3D geological analysis of Gusev Crater and surrounding terrain resulted in a geological map (Fig. 1) and geological cross-sections (Fig. 2).

We distinguished three different geological terrains, each consisting of a number of geological units: the Highland terrain (including the deposits related to Ma'adim Vallis), the Lowland terrain and the terrain interior to Gusev Crater. The stratigraphy and geological relationships between

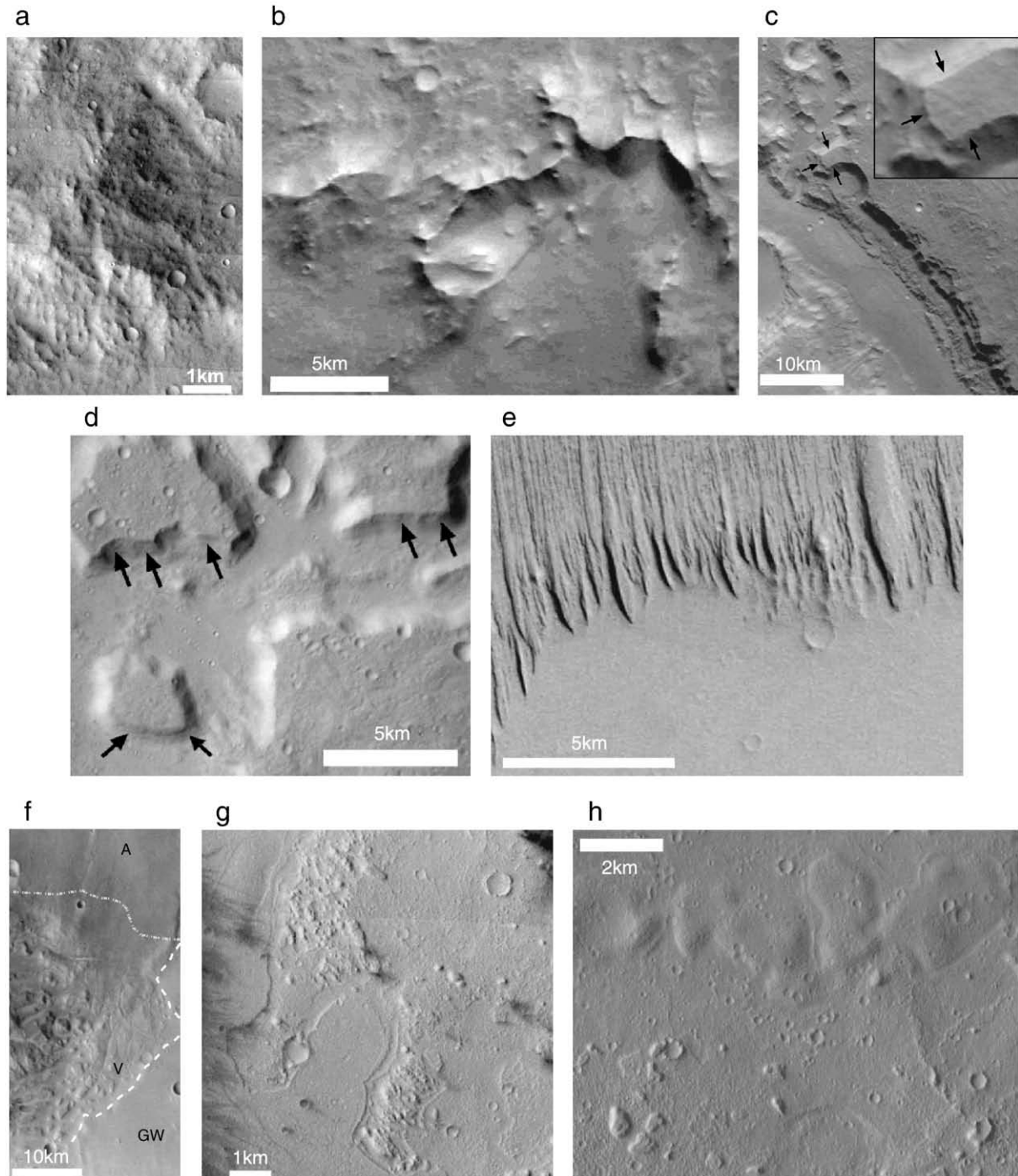


**Fig. 3.** Characteristic images of the different units, image locations are indicated on Fig. 1a. a, b and c) Characteristic images of the rugged terrain and mountainous areas of the highlands surrounding Gusev a) sub-image from THEMIS visible image V07859003; b and c) sub-images from HRSC orbit 283. c) illustrates the incision of Ma'adim Vallis in the surrounding highlands and exposing horizontal layering. d) sub-images from THEMIS visible image V01942003 showing mesas of Ma'adim Vallis Formation, arrows indicate horizontal layering within the mesas. e and f) Characteristic images of the lowland terrain north of Gusev Crater e) boundary between the Medusae Fossae Formation in the north and Galdakao Formation in the south, sub-image from HRSC orbit 335 f) boundary between the Vaucouleurs- (V), Apollinaris (A) Formation and Galdakao West (GW) Formation (grey dotted line) and Vaucouleurs- and Galdakao West Formation (white dotted line) sub-image from HRSC orbit 24. The boundary between the Vaucouleurs- and Apollinaris Formation is gradual and shows no change in relief. However, the boundary between Vaucouleurs- and Galdakao West Formation is characterised by relative large relief differences. g and h) Characteristic images of the units within Gusev Crater g) boundary between Thira West- and Thira East Formation, showing the lobate character of the former and etched appearance of the latter, sub-image from THEMIS visible image V0158003 h) gradual transition of Thira East- and Thira North Formation, subdued ridges are characteristic for the Thira North Formation, sub-image from THEMIS visible image V05662001.

units and terrains is described below. For an overview of characteristics of different units and members in units see [Table 1](#).

The highlands in the study area ([Fig. 3a–c](#)) are dominated by rugged terrains showing abundant small and large impact craters. The large impact craters displayed relatively flat and smooth crater floors, which were subsequently mapped as potential impact sheets. The highlands are geologically complex, show thick horizontal layering ([Fig. 3c](#)) and have abundant erosional features, such as grooves and channels. There are some mountainous areas present in the highlands ([Fig. 3b](#)), they are elevated up to ~2 km above the surrounding highlands and possibly include strato volcanoes ([Greeley and Spudis, 1978](#); [Stewart and Head, 2001](#)). We mapped the highlands in the region as a single unit in which two members were distinguished: the Gusev Highland Member and the Modified Gusev Highland Member. The Modified Gusev Highland Member generally shows fewer impact craters and channels, and typically fills topographic lows formed by the Highland member.

Ma'adim Vallis dissects the highlands, exposing various levels ([Fig. 3c](#)), and enters Gusev Crater from the south. Topographic data indicates that the valley reaches depths of ~2 km, which is hence the minimum thickness for the highlands. Including the thickness of the mountainous areas provides us with a thickness estimate of the highlands of several kilometres. The highlands are therefore the thick basement, shown in cross-section in [Fig. 2a](#), and most widespread unit in the Gusev Crater region.

Ma'adim Vallis Formation consists of two members: the flat topped mesas within Gusev Crater and the valley floor ([Fig. 1](#)), the age relationship with Gusev Crater Formation is not clear. Based on morphology, Gusev Crater Formation appears to embay Ma'adim Vallis Formation, which would imply a younger age of the former ([Fig. 2a, b](#)). However, based on these observations we cannot exclude that Ma'adim Vallis Formation is superposed on Gusev Crater Formation. Layers are observed within the mesas ([Fig. 3d](#)) standing as high as ~450 m above the crater floor ([Fig. 2a](#)). The current height of the mesas thus serves as minimum thickness for Ma'adim Vallis Formation.

The general morphology of the lowlands is characterised by large variations in overall relief. The lowland units show fewer signs of surface modifications such as grooves, channels and impact craters compared to the highlands. Six lowlands units are mapped. [Fig. 3f](#) shows part of the Zutphen-, Galdakao West- and Vaucouleurs Formation and [Fig. 2b](#) and [c](#) show cross-sections through the lowlands, illustrating stratigraphic relationships between the various units and relief changes along the Galdakao West- and Vaucouleurs Formation boundary. The boundary between the Vaucouleurs- and Apollinaris Formation is gradational and there is no relief difference apparent ([Fig. 3f](#)). The boundary between Vaucouleurs- and Galdakao West Formation, however, is more distinct, since it is characterised by a break of slope. [Fig. 2b](#) is a SE–NW profile through the northern rim of Gusev Crater, and shows the relationship between the Zutphen-, Galdakao West- and Vaucouleurs Formations, which become stratigraphically thicker towards the SE. The Zutphen Formation ranges in thickness from a few hundred meters southeast of Zutphen Crater to 1500 m, west of Galdakao Crater. The surface of the Zutphen Formation is characterised by a varying amount of grooves and/or channels, increasing in frequency towards the Zutphen- and Galdakao impact craters. Towards the west Zutphen Formation has a smoother surface, with more localised undulations. No layering is observed in the steep slopes on the boundary between the Zutphen- and Galdakao Formation or in small craters present. [Fig. 2c](#) is a SW–NE cross-section illustrating the stratigraphic relation between the Galdakao West-, Vaucouleurs- and Apollinaris Formations. Both Galdakao West- and Apollinaris Formations are stratigraphically superposed on the Vaucouleurs Formation. This implies that the Vaucouleurs Formation is older than both the Galdakao West- and Apollinaris Formation. The Vaucouleurs Formation consists of elevated knobs and mesas that

occur in groups or as isolated features, commonly known as chaotic terrain ([Sharp, 1973](#)). The features range in size from 1 to 10 km across, and occupy a significant part of de Vaucouleurs Crater.

Galdakao East- and Galdakao West Formation are relatively flat, have a prevalent smooth appearance, with locally subdued ridges present and are characterised by relatively low thermal inertia. Galdakao East Formation is additionally characterised by the local presence of buttes and mesas. Night temperatures for the Galdakao East Formation are lower indicating that the surface is covered primarily by dust.

The Medusae Fossae Formation is not included in the cross-sections, but is superposed on the Galdakao East Formation ([Fig. 3e](#)). The Medusae Fossae Formation is characterised by narrowly spaced ridges, or yardangs, with an overall north–south orientation ([Fig. 3e](#)) and are thought to represent wind related erosion ([Scott and Tanaka, 1986](#); [Greeley and Guest, 1987](#); [Bradley et al., 2002](#)), possibly sourced by volcanic air fall products.

Five different units characterise the floor of Gusev Crater, including part of the Ma'adim Vallis Formation. Part of the Gusev Crater floor exhibits a characteristic low albedo, coinciding with dust devil tracks, LA<sub>f</sub> ([Milam et al., 2003](#)) and LA unit ([Martinez-Alonso et al., 2005](#)). Several lines of evidence suggest that these regions are the result of removal of higher albedo dust and their pattern shows redistribution with time ([Milam et al., 2003](#)). Photometric analysis ([Jehl et al., 2008](#)) shows that the low albedo regions are relatively dust free.

The Gusev Crater Formation is largely flat, occupies most of the western crater floor ([Greeley et al., 2005](#)) and coincides largely with previously described plains ([Milam et al., 2003](#)) and plain materials ([Martinez-Alonso et al., 2005](#)). The surface is generally smooth despite the local presence of ridges and craters. Present ridges have a similar appearance to those within the Galdakao Formations. No apparent layering is observed within Crivitz, the largest crater present within Gusev Crater Formation, excavating the formation to deeper levels. The craters within this formation have unique thermophysical characteristics ([Table 1](#), see also [Milam et al., 2003](#)). The contact with the northern crater wall is characterised by mare like ridges (“wrinkle ridges”). Because of limited topographic variations of the Gusev Crater floor, the thickness of Gusev Crater Formation cannot be accurately determined. From detailed geologic cross-sections ([Fig. 2a, b](#)) we estimated a thickness of minimum 150 m (MOLA: –1810 m down to –1960). If we assume that Gusev Crater Formation extends to the depth of Crivitz Crater (MOLA: –2260) the thickness would at least be 350 m.

The Columbia Hills, studied in detail by Spirit Rover (e.g. [Squyres et al., 2006](#); [Clark et al., 2007](#)) have not been mapped as an individual unit, because the outcrop is too small for the scale on which we mapped the region. However, the (variable) characteristics are distinct from the surrounding units that we and others have mapped ([Kuzmin et al., 2000](#); [Milam et al., 2003](#); [Martinez-Alonso et al., 2005](#)), both in composition (e.g. [Golombek et al., 2006](#); [McSween et al., 2006a](#)) and bedding tilt ([McCoy et al., 2008](#)). The Columbia Hills are embayed (e.g. [Fig. 11d](#), [Martinez-Alonso et al., 2005](#)) and therefore an angular unconformity exists with the Gusev Crater Formation.

The eastern half of Gusev Crater is dominated by three formations, located around Thira impact crater: the Thira West-, Thira East- and Thira North Formation. The units are relatively flat but at least 80, 200 and 100 m thick respectively. Because of the low relief on the floor it is not possible to determine a reliable stratigraphic relationship between the various units. Thira West Formation is present within and west of Thira Crater and coincides closely with the previously described lobate unit by [Milam et al. \(2003\)](#) and partially with the high thermal inertia smooth unit ([Martinez-Alonso et al., 2005](#)). The surface is relative smooth at HRSC and THEMIS visible resolution, but MOC images reveal numerous small, 10–20 m across, pits, isolated or present in clusters. The surface is further characterised by small, simple, heavily degraded craters. The boundary between Thira West-

and Thira East Formation is characterised by layered ‘lobes’, of the former extending towards the Thira East Formation (Fig. 3g). Comparing these features to terrestrial Hawaiian lava flows Martinez-Alonso et al. (2005) suggested that the formation is a basaltic lava flow. Thira East Formation is comparable to the etched (Milam et al., 2003) and partially to the high thermal inertia rough unit (HTIR, Martinez-Alonso et al., 2005), has a rough, heavily etched and pitted appearance. Locally smoother patches exist, primarily surrounding impact craters of a few hundred meters across. MOC images reveal knobs and small buttes, with an apparent northwest–southeast direction. West in the Gusev Crater a small area was also mapped as the Thira East Formation. Martinez-Alonso et al. (2005) additionally suggested that a small outcrop of the HTIR unit occurs south of Columbia Hills (e.g. Fig. 11d, Martinez-Alonso et al., 2005). Similar to the relationship with Gusev Crater Formation the HTIR unit appears to embay the Columbia Hills.

Thira North Formation (Fig. 3h) partly coincides with the wrinkled (Milam et al., 2003) and low thermal inertia unit (Martinez-Alonso et al., 2005). It is dominated by undulations of various sizes consisting of small scale ridges. Ridges are partially subdued, narrow, a-symmetric, and trend mostly in a northeast–southwest direction. The larger more prominent ridges do not appear to show a preferred orientation.

We studied the boundaries between the units in detail, in an attempt to unravel the stratigraphic relationships. Superposition of the lobate margins of the Thira West Formation suggest that this unit is geologically younger than Thira East Formation, as noted previously (Milam et al., 2003; Martinez-Alonso et al., 2005). However, as shown in the next section, this is inconsistent with crater count ages. This can potentially be explained by the hypothesis of Gregg et al. (2007) in which Thira East Formation was covered by ice rich deposits, against which Thira West Formation basalts abutted. The subsequent sublimation of ice from Thira East Formation could have resulted in the hummocky appearance and apparent younger (resurfaced) surface age.

Stratigraphic relations between Thira West- and Thira North Formation and between Thira West- and Thira East Formation suggest that the Thira North Formation is the oldest of the three.

#### 4.2. Crater count ages and implications

Surface areas representative for each unit (Fig. 4a, Table 1), were selected for crater counts to determine surface ages. We compared and integrated these with our stratigraphic relations to provide a relative timescale for the geological evolution of the Gusev Crater region (Fig. 5). In general crater count ages do not provide the age of the unit, but rather the minimum age of the surface; for example, erosion processes can result in younger ages of the surface than that of the rock unit. Moreover crater counts ages are generally limited in accuracy by statistical error (Neukum et al., 2001). Results of the crater count ages (Appendix A) are shown in Table 1 and Fig. 4b. Although crater ages for the Vaucouleurs- and Medusae Fossae Formation were not directly determined, the age of the Vaucouleurs Formation is constrained by the overlying Galdakao West- and Apollinaris Formation and is older than  $3.85 \pm 0.15$  Ga, while the age of the Medusae Fossae Formation is constrained by the surface age of the ejecta blanket of an unnamed crater (number 12 on Fig. 4a) to be older than  $1.13 \pm 0.56$  Ga.

Galdakao Formation was initially mapped as a single unit based on its overall appearance. However, crater counts revealed two distinct ages for the western and eastern half of the formation of  $3.85 \pm 0.15$  Ga and  $3.57 \pm 0.06$  Ga respectively. Since there is no overlap in error, the eastern and western half are considered to represent two stages of possibly a similar process of deposition. Images show no significant morphological differences between the areas, except the presence of buttes and mesas in the eastern half. However, an average relief difference of 200 m, lower for the eastern half is apparent. Additionally the Galdakao West Formation

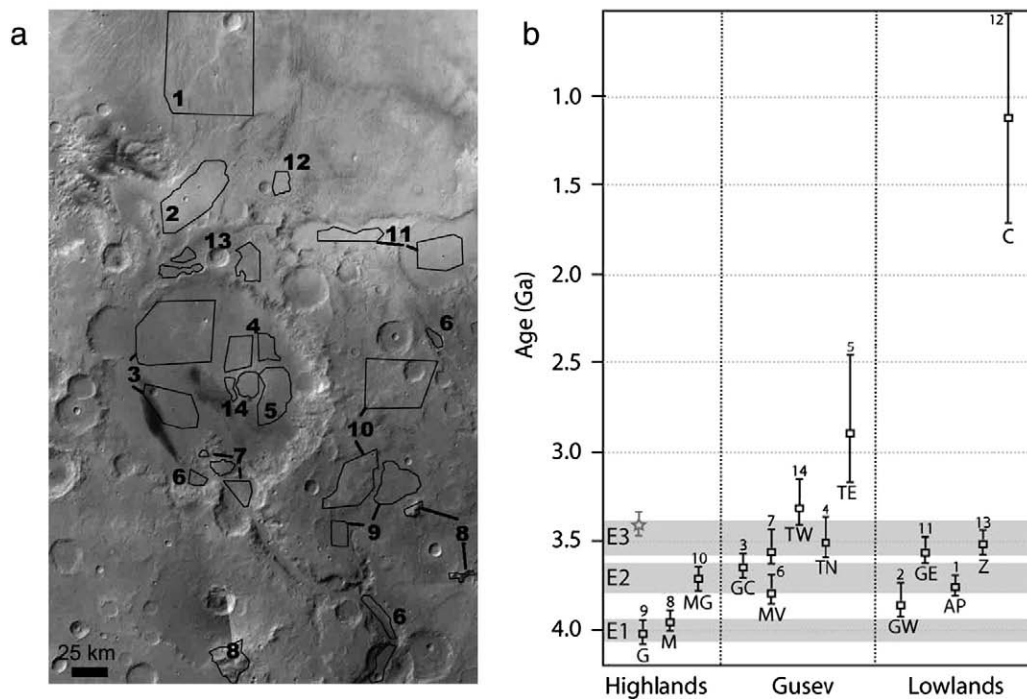


**Fig. 4.** Crater count ages. a) Overview of selected areas used for age determination using crater counts, background is a MOC wide angle mosaic. The following areas were studied (numbers refer to the area, abbreviations refer to the formation specified in panel b) for the highland Formation: M— Mountainous member (8), MG— Modified Gusev member (9) G— Gusev Highland member (10); for the lowland units: AP— Apollinaris Formation (1), GW— Galdakao West Formation (2), GE— Galdakao East Formation (11), C— unnamed crater (12), Z— Zutphen Formation (13); for the units within Gusev Crater: GC— Gusev Crater Formation (3), TN— Thira North Formation (4), TE— Thira East Formation (5), MV— Ma’adim Vallis Formation (6 and 7), TW— Thira West Formation (14). b) Summary of ages determined via crater statistics. Abbreviations and numbers as in Fig. panel a. The grey areas refer to three episodes of increased activity at 4 Ga, 3.7 Ga, and 3.5 Ga, marked E1, E2 and E3 respectively.

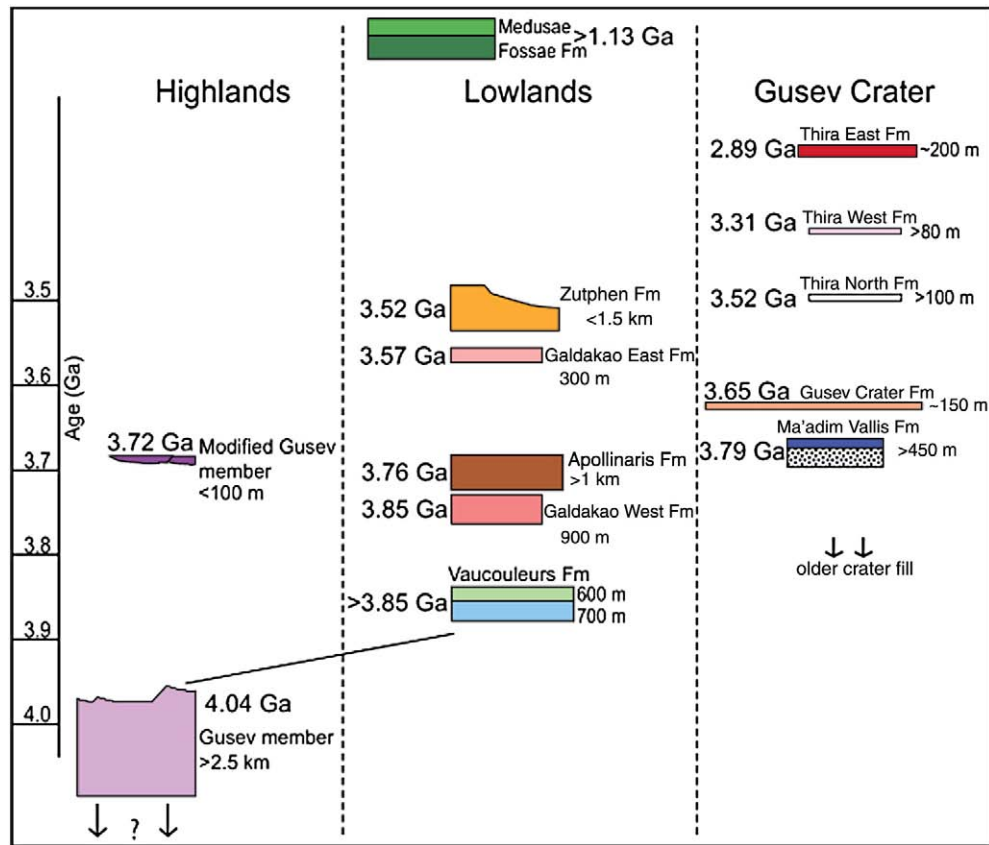


Fig. 5. Stratigraphy of the Gusev Crater region, including unit thicknesses and crater count ages.

indicates a resurfacing event at  $2.43^{+0.58}_{-0.64}$  Ga (Appendix A), whereas the Galdakao East Formation does not.

Three main episodes are defined for the geologic events for the region (Fig. 4b). The first episode (4.05 to 3.95 Ga) is related to the widespread formation of the highlands. Crater ages confirm that the Highland Formation is the oldest unit in the area at  $4.04^{+0.06}_{-0.10}$  Ga. The second episode (3.77 to 3.65 Ga) relates the deposition of the Modified Gusev Highland Member, Apollinaris- and Gusev Crater Formation. Earlier studies (McSween et al., 2004; Martinez-Alonso et al., 2005; Greeley et al., 2005; Golombek et al., 2006) showed that Spirits' landing site and hence Gusev Crater Formation ( $3.65^{+0.06}_{-0.10}$  Ga) is basaltic in composition. It is likely that this second episode represents widespread basaltic eruptions including emplacement of the Apollinaris Formation. This implies that topographic lows of the highlands, the Modified Gusev Highland Member were filled during a general period of volcanic activity, possibly involving fissure style eruptions. Even though the surface age of Galdakao West Formation is dated slightly older, we propose that it could also be related to this second, widespread 3.7 Ga basaltic volcanic episode, since there is a strong morphological resemblance between Galdakao East-, Galdakao West- and Gusev Crater Formation.

As mentioned, Galdakao West- and Apollinaris Formation lie stratigraphically above Vaucouleurs Formation. This implies an older age for the Vaucouleurs Formation, e.g. older than the deposition of Apollinaris Formation at  $3.76^{+0.04}_{-0.06}$  Ga and Galdakao West Formation at  $3.85^{+0.15}_{-0.15}$  Ga. The deposition and subsequent deformation and 'chaotization' of Vaucouleurs Formation thus occurred before deposition of both the Apollinaris- and Galdakao West Formation. This is consistent with a link between the chaotization event and volcanic activity suggested by Robinson et al. (1993).

Image data and resulting cross-section (Fig. 2a) suggest the superposition of the Galdakao West Formation on the Apollinaris

Formation. The crater count surface ages of the two units are within error of each other, so relative ages cannot be distinguished based on surface age.

The third and final episode (3.58 to 3.41 Ga) is related to resurfacing of the Gusev Highland Member, the deposition of Thira North-, Galdakao East- and Zutphen Formation, and postdates the final episode of activity of Apollinaris Patera. Zutphen Formation has an age of  $3.52^{+0.05}_{-0.08}$  Ga and cross-sections (Fig. 2a and b) indicate that this unit lies stratigraphically on Galdakao West Formation, consistent with the younger crater count age. The three formations deposited during this episode do not show any clear connection to known episodes of volcanism in the region. The morphological resemblance between the Galdakao Formations and Gusev Crater Formation could imply that the Galdakao East Formation is also sourced by basaltic volcanism. This could indicate a localised source responsible for deposition of these three formations.

As mentioned, crater count ages of units within Gusev Crater differ from apparent stratigraphic relationships, possibly due to varying degrees of erosion within units. The oldest unit mapped within the crater is Gusev Crater Formation, which occupies a significant part of the crater's floor. Stratigraphic relations indicate that Thira North Formation is older than both Thira West- and Thira East Formations, crater counting confirms this and suggest an age of  $3.52^{+0.08}_{-0.16}$  Ga for Thira North (similar to Zutphen Formation). Crater count ages for Thira East- and Thira West Formation are  $2.89^{+0.28}_{-0.44}$  Ga and  $3.31^{+0.09}_{-0.17}$  Ga respectively.

Deposition of Ma'adim Vallis Formation is not linked to any of the three defined geologic episodes. Crater count ages for Ma'adim Vallis reveal two ages:  $3.79^{+0.05}_{-0.08}$  Ga for the valley floor areas, and  $3.58^{+0.06}_{-0.10}$  Ga for three mesas. It is difficult to reconcile these ages with the geological sequence of events. We expect the valley floor surface age to record the most recent putative fluvial activity with a strong erosional component, or possibly a windblown mantling

deposit whereas the mesas may represent an older unit, deposited at the outlet of Ma'adim Vallis, potentially a fan or delta deposit that formed quickly, during an earlier or possibly during the final stage of fluvial activity. This contradicts with the surface ages. Since the mesas have a positive topography with respect to the floor of Gusev Crater and Ma'adim Vallis, we consider it likely that the mesas suffered considerable erosion, such that the crater count age of the surface does not necessarily reflect the actual age of the unit implying that the mesas could be  $\geq 3.79$  Ga.

## 5. Discussion

The geologic map and geological analysis based on the cross-sections and crater ages are in general agreement with earlier studies, based on Viking (Kuzmin et al., 2000) and THEMIS (Milam et al., 2003; Martinez-Alonso et al., 2005) data. However, in a number of areas the approach used here provides new insights into the geologic evolution of the Gusev Crater region. The new insights that we gained are primarily derived from our 3D structural geological analysis. Combining the geologic mapping and cross-sections we now have a strong constraint on superposition relations of many of the mapped units, as well as thickness estimates. The crater count surface ages serve to bracket the timeframe during which deposition and surface modification of units took place. From this combination of 3D geological information and age estimates we derived a detailed sequence of events for the region.

### 5.1. Sequence of geologic events

The main activity within the Gusev Crater region was restricted to three episodes at  $>4$  Ga, 3.7 Ga, and 3.5 Ga (Fig. 4b). The highland unit is the oldest recognised unit with a surface age of  $\sim 4$  Ga. In detail (and beyond the scope of this paper), the highlands show a complex geology, in which several sub-units can be distinguished. The highlands also show abundant erosional features, attesting to a more dynamic surface environment in the period prior to 4 Ga. The 4 Ga surface age is in the case of the highlands clearly a younger, lower limit, to the actual ages of the geological units making up the highland terrain, which is at least 2.5 km thick.

The lowland units were mostly deposited during the 3.7 and 3.5 Ga episodes, with the youngest unit being the Medusae Fossae Formation. At least parts of the lowland deposits (e.g. Gusev Crater- and Galdakao Formation), are likely linked to Apollinaris Patera volcanism at  $\sim 3.7$  Ga. The Vaucouleurs Formation has a minimum age constraint imposed by deposition of Galdakao West- and Apollinaris Formation of 3.8 Ga. The most likely scenario is that the original deposition of units in the Vaucouleurs Crater was coeval to part of the formation of the Highland terrain at  $>4$  Ga. The break-up of these units into the present chaotic terrain occurred prior to, or during the 3.7 Ga event. The chaotization event may have been related to the same thermal event that resulted in the 3.7 Ga volcanism. Considering the ages of the Apollinaris Patera volcanics, Apollinaris- ( $3.76^{+0.04}_{-0.06}$  Ga) and Galdakao West Formation ( $3.85^{+0.15}_{-0.12}$  Ga) it is possible that Galdakao West Formation represents volcanic material from an earlier stage of Apollinaris Patera.

The Zutphen Formation occupies the northern rim of the Gusev Crater. It is as thick as 1.5 km and is hence a significant deposition at  $3.52^{+0.05}_{-0.08}$  Ga. As noted in the previous section its deposition could be related to Thira North Formation at  $3.52^{+0.08}_{-0.16}$  Ga. However there does not seem to be any direct morphological similarities between the two formations. The grooves and channels characterising the surface of the Zutphen Formation must have formed after deposition, e.g. later than  $3.52^{+0.05}_{-0.08}$  Ga.

A comparison of Gusev Crater with similar sized 'fresh', unfilled craters, follows in the next section, suggesting that the original level of Gusev Crater floor could have been in the order of 1500 m deeper than the current level. Gusev Crater Formation is estimated to be minimum

150 m thick and thus probably does not fully account for the fill sequence. The original crater basin must have been filled initially by impact related materials, such as an impact melt sheet, impactites and subsequently by putative sediments from Ma'adim Vallis, which could in fact account for a fair amount, up to 1 km (Hauber et al., 2009). The minimum thickness of 450 m estimated for Ma'adim Vallis Formation is based on the height of the mesas, and could thus be significantly thicker. Crater count statistics of the mesas indicate a final stage of fluvial activity at  $3.58^{+0.06}_{-0.10}$  Ga relating to the formation of the mesas. We argue that this cannot have been the case, since the formation of the mesas requires vast amounts of material to be released inside Gusev Crater. We expect that the mesa crater count age is in fact an erosional age, particularly considering that the Gusev Crater Formation, which embays the mesas, is apparently older (3.65 Ga). The other formations present within the crater are, based on crater statistics, all dated younger than the widespread Gusev Crater Formation,  $3.65^{+0.06}_{-0.10}$  Ga. The Columbia Hills are too small for crater counting, but stratigraphic relationships suggest that an angular unconformity exists with the surrounding units embaying Columbia Hills.

### 5.2. Geometry of the Gusev Crater

The geometry of Gusev Crater is particularly interesting since the craters' size suggests that it should be a complex impact crater. However, a central uplifted region has not been identified. A logical question that follows is: Has subsequent volcanism and perhaps sedimentation covered and obscured the craters' central uplift?

The Gusev Crater has a rim-to-rim diameter of  $\sim 160$  km and floor to floor diameter of  $\sim 120$  km. A number of impact craters with rim diameters  $100 < D < 180$  km (Table 2) were selected to serve as a

**Table 2**  
Selected Martian craters for comparison with Gusev Crater.

Crater name	Lat. °*	Long., °E*	D, (km)*	$D_a$ , (km)**	$H_a$ , (m)**	$d_{SM}^{**}$	$H_a$ , (m) for filled craters
Green	-52.7	351.6	184	170	1800	1200	
Molesworth	-27.7	149.1	181				
Baldet	23	65.4	180				1800
Terby	-28.3	74.1	174				1240
Flammarion	25.4	48.2	173				1500
Wallace	-52.9	110.6	173				1130
Becquerel	22.3	352	171.2				1200
Henry	10.9	23.3	171				
Proctor	-48	29.5	168.2				700
Gusev	-14.7	175.4	166	150			1100
Bakhuysen	-23.3	15.6	161	150	2600	1400	
Schaeberle	-24.7	50.1	160				700
Janssen	2.7	37.5	158				1400
Lohse (Fig. 6a)	-43	343	156	150	2800	1500	
Holden	-26.4	326	153.8	150	2400	1300	
Lomonosov	65.2	350.8	153	110	1900	1500	
Hale	-36.1	323.5	149	130	2800	1300	
Quenisset	34.3	40.6	138	125	1500	900	
Moreux	41.8	44.4	138	120	2200	400	
Liu_Hsin	-53.3	188.4	137	130	1800	-500	
Cerulli	32.2	22.1	130	110	2800	1400	
Maraldi	-62	328	124	120	2100	1500	
Milankovivc	54.7	213.4	118	110	1800	1000	
Fournier	-4.3	72.6	118	105	1700	1000	
Wright	-58.6	209	115	110	1200	-400	
Perrepelkin	52.5	295.4	112	80	1700	700	
Mie	48.1	139.6	104	100	1400	1000	
Du Martheray (Fig. 6b)	5.5	93.5	102	90	2100	500	

\*Latitude, longitude and rim crater diameter are according to JMars-related databases.

\*\*Apparent diameter  $D_a$ , depth  $H_a$ , and depth of the central mound summit  $d_{SM}$  are measured in respect to estimated pre-impact surface. Due to rough surface depth estimates seems to have error bars of the order of  $\pm 100$  m.

comparison to the Gusev Crater. Some of these craters, including Gusev, have relatively flat floors apparently due to infilling by post-impact sediments and/or volcanic materials. The apparent depth of

the flat floor of these craters is listed in the last column of Table 2. A second group of craters, also partially filled with post-impact sediments and/or volcanic materials does have a relatively distinct

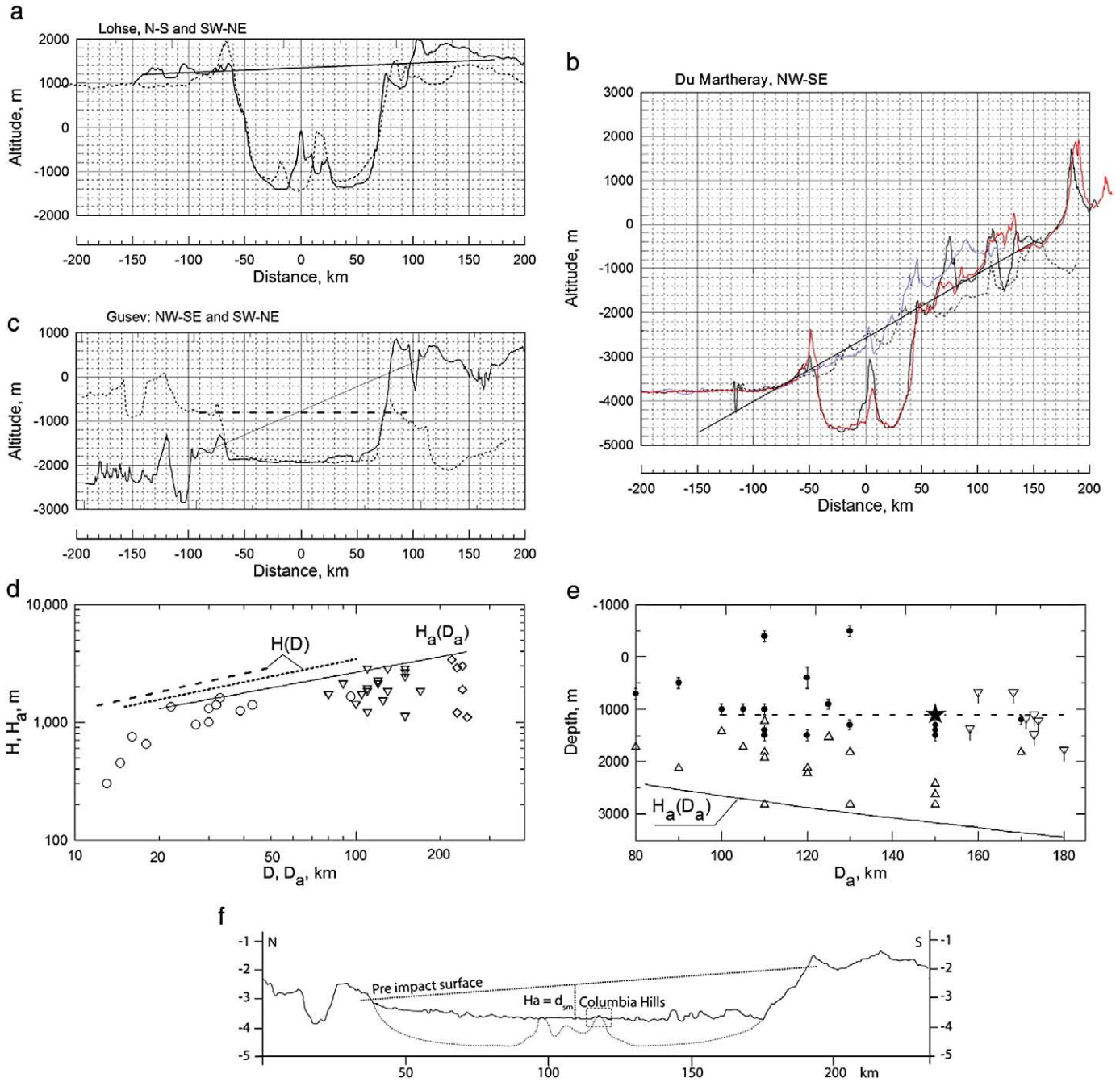


**Fig. 6.** Comparison of Gusev Crater and pristine craters of similar size. a) Two topographic profiles through the centre of Lohse crater (solid curve is for N–S direction, dashed curve is for SW–NE direction). Black line shows an approximated pre-impact surface in N–S direction. The central uplift region is clearly visible. b) A set of NW–SE profiles through the central summit and outside the Du Martheray crater demonstrates that in an oblique surface ( $\sim 1400$  m per 100 km) the central mound may be at the level of lowest rim portion but well below ( $\sim 1$  km) the highest rim portion. c) Two profiles through Gusev Crater (NW–SE – solid curve, SW–NE – dashed curve) show an apparent gradient  $\sim 1100$  m per 100 km in the NW–SE direction. With respect to the more level SW–NE direction, the flat floor depth is about 1100 m below the pre-impact surface. The crater rim elevation in NW area is  $\sim 600$  m above the floor while in the SE portion the rim elevation is about 2600 m above the floor. d) Depth–diameter relations for Martian impact craters in log–log coordinates. For craters smaller 100 km in diameter a set of analytic relations is published for rim-crest diameters  $D$  and the depth below the rim crest  $H$ : dotted line is after Garvin et al. (2003), dashed line is after Boyce and Garbeil (2007) who measured most pristine craters. Authors’ selected data (circles for small craters, downward triangles for large craters and diamonds for basins with  $D > 1$  km) are obtained with estimation of the pre-impact surface position and present “apparent” depth and diameters. Craters with largest apparent depth can be “covered” with the curve  $H_a(m) = 350 * D_a^{0.44}$  which gives us the best available estimate for the apparent depth of “pristine” craters. e) Linear plot of data in Table 2 of apparent diameter ( $D_a$ ) vs. Depth ( $H_a$ ). Note that vertical axis is directed downward. Black dots with error bars show the summit of the central mound position below the assumed pre-impact surface,  $d_{SM}$ . Upward triangles show apparent depths for craters in Table 2. Downward triangles show apparent depth for heavily filled craters in Table 2 where no central mounds are visible. These points present the “upper limit” to the  $d_{SM}$ . Black star is for Gusev average apparent depth of 1100 m (see panel c for details), the same level is outlined with the horizontal dashed line. The solid curve is a fragment of  $H_a(D_a)$  relationship shown in panel d). f) Sketch of suggested situation for Gusev Crater in cross-section, based on the above estimate for the Gusev central mound geometry. The top of the original central mound is just visible above the infill of Gusev Crater and thought to represent Columbia Hills.

central mound rising above the crater floor. For this latter group the “apparent depth” and “depth of the central mound summit ( $d_{SM}$ )” were measured in respect to the estimated pre-impact surface. These are measured using topographic profiles across various craters on Mars combined with JMars software (Fig. 6a). We assume that the visible central mound in our selection of craters is the remnant of the real central mound, formed during collapse of the central cavity.

In many cases pre-impact surface topography is variable, with topographic slopes up to 1000–2000 m per 100 km (Fig. 6b), which is comparable with the final crater depth. Gusev Crater belongs to this subsample (Fig. 6c). The average depth is  $\sim 1$  km, but rim elevations range up to 3 km.

The data are summarised in Fig. 6d and e. Fig. 6d shows apparent depths of measured craters in the context of other published depth–diameter relations (mostly for rim–crest diameters and the depth below the rim–crest level). Fig. 6e shows data for apparent crater depths and central summit position for craters in Table 2. For craters with diameters from 100 to 180 km there is no evident trend in  $d_{SM}(D_a)$  dependence: the cloud of  $d_{SM}$  dots occupy the area of  $d_{SM} \geq 1500$  m.

Comparison of Gusev Crater with these similar sized craters (Table 2) shows that some of the craters do show central uplifts, whereas others, including Gusev, do not. The lack of central uplifts is apparently due to infilling by post-impact materials and peak erosion over time. A few craters have their central peak rising above the pre-impact surface level. Three craters with apparent diameters of  $\sim 150$  km similar to Gusev Crater have central peak summits just below the apparent depth of Gusev Crater of 1100 m.

Taking into account (a) the natural scatter of  $d_{SM}$  values and (b) the specific of the central mound position in a rough or oblique-surface terrains (like in Fig. 6b) we should not exclude the possibility that the modern level of Gusev’s visible floor is close to the central peak summit position. The Columbia Hills could be a remnant of the pristine central uplift and/or early deposits covering the structural uplift (Fig. 6f). This is consistent with findings of McCoy et al. (2008) who analysed the 3D geometry of the Columbia Hills by using dips measured by MER Spirit. Other hypothesis for the origin of Columbia Hills include erosional remnant of layered material, volcanic construct, or a tectonic wrinkle ridge (Rice, 2005) appear less likely. Additionally compositional analysis by Spirit, showing that rocks within Columbia hills are highly phosphorous and hydrothermally altered (e.g. Squyres et al., 2006) agree with the expectations for centrally uplifted regions of complex impact craters.

### 5.3. Gusev Crater regional events in the global context

From a variety of sources of information it is clear that the geologically most active period in Mars history was the Noachian and early Hesperian (Head et al., 2001; Solomon et al., 2005 and references therein; Bibring et al., 2006). The Gusev Crater region is no exception, with deposition of all units, except the Medusae Fossae Formation, prior to 3.5 Ga. Mineralogical evidence, in the form of phyllosilicates, morphological evidence and evidence from the only Noachian Martian meteorite, Allan Hills 84001 (Nyquist et al., 2001), all suggest interaction of the Martian crust with liquid water in the period prior to 4 Ga. This is consistent with formation of the highland terrains in the Gusev Crater region in a geologically most active and ‘wet’ period, involving relatively high erosion rates.

The impact that formed Gusev Crater must have taken place after 4.0 Ga (lower limit of the Highland Formation) and before 3.8 Ga (onset of deposition of units within Gusev Crater), coinciding with the waning stages of the Late Heavy Bombardment event (e.g. Gomes et al., 2005).

Most of deposition in Gusev Crater, with an estimated thickness of 1500 m, must have taken place prior to the emplacement of the Gusev Crater Formation at 3.65 Ga. Gusev basin fill may include sediments transported by Ma’adim Vallis’ and volcanic sequences perhaps

associated with Apollinaris Patera. Globally, this period is characterised by magmatic events associated with the build-up of Tharsis and smaller volcanic edifices, such as Apollinaris Patera. Activity of outflow channels appear to follow the major volcanic events (Neukum et al., 2010–this issue) and this also appears to be the case for the Gusev Crater region.

According to our geometric analysis the Columbia Hills could represent a relict of the original central uplift of Gusev Crater. This would imply that the rock units analysed by the MER rover were formed prior to the impact that created Gusev Crater, and have been heavily deformed and altered during and directly after the impact event (McCoy et al., 2008).

Bibring et al. (2006) proposed an association of the  $\sim 3.7$  Ga volcanic event with deposition of sulphate deposits, typically found in light toned layered sequences. In the Gusev Crater region we have no indication for the presence of sulphate bearing deposits in the units formed at  $\sim 3.7$  Ga. However, detailed studies of hyperspectral data using OMEGA or CRISM data sets have not been carried out.

In the Gusev Crater and on the northern rim we find units deposited at  $\sim 3.5$  Ga. Those units appear to post-date the major volcanic event at  $\sim 3.7$  Ga. The most voluminous of those units is the Zutphen unit, with a thickness up to 1.5 km. It is not clear what the composition and depositional process of these deposits is.

## 6. Conclusions

The main activity within the Gusev Crater region is restricted to three episodes at  $> 4$  Ga, 3.7 Ga and 3.5 Ga. The record of geological events in the Gusev Crater region can be linked to global Martian events and place additional time constraints on such events. The geometry of the Gusev Crater as compared to similar sized Martian craters could indicate that the Columbia Hills represent a relict of the central uplift of the crater.

## Acknowledgements

We like to thank the HRSC CO-I team for providing the DEM’s. We would like to thank Sara Martinez-Alonso and an anonymous reviewer for their comments and suggestions, which significantly improved the manuscript. We also would like to thank S. Parker, J. Chadwick, R. Greeley and M. Kleinbans for providing useful comments to the manuscript.

## Appendix A. Supplementary data

Supplementary data associated with this article can be found, in the online version, at doi:10.1016/j.epsl.2010.01.013.

## References

- Bibring, J.P., Langevin, Y., Mustard, J.F., Poulet, F., Arvidson, R., Gendrin, A., Gondet, B., Mangold, N., Pinet, P., Forget, F., the OMEGA team, 2006. Global mineralogical and aqueous Mars history derived from OMEGA/Mars Express data. *Science* 312, 400–404.
- Boyce, J.M., Garbeil, H., 2007. Geometric relationships of pristine Martian complex impact craters, their implications to Mars geologic history. *Geophys. Res. Lett.* 34, 16.
- Bradley, B.A., Sakimoto, S.E.H., Frey, H., Zibelman, J.R., 2002. Medusae Fossae Formation: new perspectives from Mars Global Surveyor. *J. Geophys. Res.* 107 (E8), 5058.
- Cabrol, N.A., Grin, E.A., Lheim, R., Kuzmin, R.O., Greeley, R., 1998. Duration of the Ma’adim Vallis/Gusev Crater hydrogeologic system, Mars. *Icarus* 133, 98–108.
- Cabrol, N.A., Grin, E.A., Carr, M.H., Sutter, B., Moore, J.M., Farmer, J.D., Greeley, R., Kuzmin, R.O., DesMarais, D.J., Kramer, M.G., Newsom, H., Barber, C., Thorsos, I., Tanaka, K.L., Barlow, N.G., Fike, D.A., Urquhart, M.L., Grigsby, B., Grant, F.D., de Goursac, O., 2003. Exploring Gusev Crater with Spirit: review of science objectives testable hypotheses. *J. Geophys. Res.* 108 (E12), 8076.
- Carter, L.M., Campbell, B.A., Watters, T.R., Phillips, R.J., Putzig, N.E., Safaeinili, A., Plaut, J.J., Okubo, C.H., Egan, A.F., Seu, R., Biccari, D., Orosei, R., 2009. Shallow radar (SHARAD) sounding observations of the Medusae Fossae Formation, Mars. *Icarus* 199, 295–302.
- Clark, B.C., Arvidson, R.E., Gellert, R., Morris, R.V., Ming, D.W., Richter, L., Ruff, S.W., Michalski, J.R., Farr, W.H., Yen, A., Herkenhoff, K.E., Li, R., Squyres, S.W., Schroder, C., Klingelhofer, G., Bell, J.F., 2007. Evidence for montmorillonite or its compositional

- equivalent in Columbia Hills, Mars. *J. Geophys. Res.* 112 (E6), E06S01. doi:10.1029/2006JE002756.
- Garvin, J.B., Sakimoto, S.E.H., Frawley, J.J., 2003. Craters on Mars: global geometric properties from gridded MOLA topography. 6th International Conference on Mars. Abstract 3277.
- Golombek, M.P., Grant, J.A., Parker, T.J., Kass, D.M., Crisp, J.A., Squyres, S.W., Haldemann, A.F.C., Adler, M., Lee, W.J., Bridges, N.T., Arvidson, R.E., Carr, M.H., Kirk, R.L., Knoke, P.C., Roncoli, R.B., Weitz, C.M., Schofield, J.T., Zurek, R.W., Christensen, P.R., Ferguson, R.L., Erson, F.S., Rice, J.W., 2003. Selection of the Mars Exploration Rover landing sites. *J. Geophys. Res.* 108 (E12), 8072.
- Golombek, M.P., Crumpler, L.S., Grant, J.A., Greeley, R., Cabrol, N.A., Parker, T.J., Rice, J.W., Ward, J.G., Arvidson, R.E., Moersch, J.E., Ferguson, R.L., Christensen, P.R., Castano, A., Castano, R., Haldemann, A.F.C., Li, R., Bell, J.F., Squyres, S.W., 2006. Geology of the Gusev cratered plains from the Spirit rover transverse. *J. Geophys. Res.* 111 (E2), E02S07. doi:10.1029/2005JE002503.
- Gomes, R., Levison, H.F., Tsiganis, K., Mordibelli, A., 2005. Origin of the cataclysmic Late Heavy Bombardment period of the terrestrial planets. *Nature* 435, 466–469.
- Gorelick, N.S., Weiss-Nalick, M., Steinberg, B., Anwar, S., 2003. JMARS: a multimission data fusion application. Lunar and Planetary Science Conference, p. 34. Abstract 2057.
- Grant, J.A., Wilson, S.A., Ruff, S.W., Golombek, M.P., Koestler, D.L., 2006. Distribution of rocks on the Gusev Plains on Husband Hill, Mars. *Geophys. Res. Lett.* 33, L16202. doi:10.1029/2006GL026964.
- Greeley, R., Guest, J.E., 1987. Geologic map of the eastern equatorial region of Mars. U.S. Geological Survey Miscellaneous Investigation Series, p. Map I-1802-B, scale 1:15M.
- Greeley, R., Spudis, P.D., 1978. Volcanism in the cratered terrain hemisphere of Mars. *Geophys. Res. Lett.* 5, 453–455.
- Greeley, R., Spudis, P.D., 1981. Volcanism on Mars. *Rev. Geophys.* 19, 13–41.
- Greeley, R., Foing, B.H., McSween, H.Y., Neukum, G., Pinet, P., van Kan, M., Werner, S.C., Williams, D.A., Zegers, T.E., 2005. Fluid lava flows in Gusev crater, Mars. *J. Geophys. Res.* 110 (E5), E05008. doi:10.1029/2005JE002401.
- Gregg, T.K.P., Briner, J.P., Paris, K.N., 2007. Ice-rich terrain in Gusev Crater, Mars? *Icarus* 192, 348–360.
- Grin, E.A., Cabrol, N.A., 1997. Limnologic analysis of Gusev Crater paleolake, Mars. *Icarus* 130, 461–474.
- Gwinner, K., Scholten, F., Spiegel, M., Schmidt, R., Giese, B., Oberst, J., Jaumann, R., Neukum, G., Team, H.C.-I., 2005. Hochauflösende Digitale Geländemodelle auf der Grundlage von Mars Express HRSC-Daten. *Photogramm. Fernerkund. Geoinf.* 5, 387–394.
- Hartmann, W.K., Neukum, G., 2001. Cratering chronology the evolution of Mars. *Space Sci. Rev.* 96, 165–194.
- Hauber, E., Gwinner, K., Kleinhaus, M., Reiss, D., Di Achille, G., Ori, G.-G., Scholten, F., Marinangeli, L., Jaumann, R., Neukum, G., 2009. Sedimentary deposits in Xanthe Terra: implications for the ancient climate on Mars. *Planet. Space Sci.* 57, 944–957.
- Head, J.W., Greeley, R., Golombek, M.P., Hartman, W.K., Hauber, E., Jaumann, E., Masson, P., Neukum, G., Nyquist, L.E., Carr, M.H., 2001. Geological processes and evolution. *Space Sci. Rev.* 96, 263–292.
- Irwin, R.P., Maxwell, T.A., Howard, A.D., Craddock, R.A., Leverington, D.W., 2002. A large paleolake basin at the head of Ma'adim Vallis, Mars. *Science* 296, 2209–2212.
- Irwin, R.P., Howard, A.D., Maxwell, T.A., 2004. Geomorphology of Ma'adim Vallis, Mars, and associated paleolake basins. *J. Geophys. Res.* 109, E12009. doi:10.1029/2004JE002287.
- Ivanov, B.A., 2001. Mars/Moon cratering rate ratio estimates. *Space Sci. Rev.* 96, 87–104.
- Ivanov, B.A., Werner, S.C., Neukum, G., 2005. Simple estimate for Gusev infilling thickness. 1st Mars Express Science Conference. Abstract 150.
- Jehl, A., Pinet, P., Baratoux, D., Daydou, Y., Chevrel, S., Heuripeau, F., Manaud, N., Cord, A., Roseberg, C., Neukum, G., Gwinner, K., Scholten, F., Hoffman, H., Roatsch, T., the HRSC Team, 2008. Gusev photometric variability as seen from orbit by HRSC/Mars-express. *Icarus* 197, 403–428.
- Kleinhaus, M.G., 2005. Flow discharge and sediment transport models for estimating a minimum timescale of hydrological activity and channel and delta formation on Mars. *J. Geophys. Res.* 110, E12003. doi:10.1029/2004JE002521.
- Kuzmin, R.O., Greeley, R., Lheim, R., Cabrol, N.A., Farmer, J.D., 2000. Geologic map of the MTM - 15182 MTM - 15187 quadrangles Gusev Crater- Ma'adim Vallis region, Mars. U.S. Geological Survey U.S. Department of the Interior, p. Map I-2666.
- Martinez-Alonso, S., Jakosky, B.M., Mellon, M.T., Putzig, N.E., 2005. A volcanic interpretation of Gusev Crater surface materials from thermophysical, spectral, morphological evidence. *J. Geophys. Res.* 110 (E1), E01003. doi:10.1029/2004JE002327.
- McCoy, T.J., Sims, M., Schmidt, M.E., Edwards, L., Tornabene, L.L., Crumpler, L.S., Cohen, B.A., Soderblom, L.A., Blaney, D.L., Squyres, S.W., Arvidson, R.E., Rice, J.W., Treguiet, E., d'Uston, C., Grant, J.A., McSween, H.Y., Golombek, M.P., Haldemann, A.F.C., de Souza, P.A., 2008. Structure, stratigraphy, origin of Husband Hill, Columbia Hills, Gusev Crater, Mars. *J. Geophys. Res.* 113 (E6), E06S03. doi:10.1029/2007JE003041.
- McSween, H.Y., Arvidson, R.E., Bell, J.F., Blaney, D., Cabrol, N.A., Christensen, P.R., Clark, B.C., Crisp, J.A., Crumpler, L.S., Des Marais, D.J., Farmer, J.D., Gellert, R., Ghosh, A., Gorevan, S., Graff, T., Grant, J., Haskin, L.A., Herkenhoff, K.E., Johnson, J.R., Jolliff, B.L., Klingelhoefer, G., Knudson, A.T., McLennan, S., Milam, K.A., Moersch, J.E., Morris, R.V., Rieder, R., Ruff, S.W., de Souza, P.A., Squyres, S.W., Wanke, H., Wang, A., Wyatt, M.B., Yen, A., Zipfel, J., 2004. Basaltic rocks analyzed by the Spirit rover in Gusev Crater. *Science* 305, 842–845.
- McSween, H.Y., Ruff, S.W., Morris, R.V., Bell, J.F., Herkenhoff, K., Gellert, R., Stockstill, K.R., Tornabene, L.L., Squyres, S.W., Crisp, J.A., Christensen, P.R., McCoy, T.J., Mittlefehldt, D.W., Schmidt, M., 2006a. Alkaline volcanic rocks from the Columbia Hills, Gusev Crater, Mars. *J. Geophys. Res.* 111 (E9), E09S91. doi:10.1029/2006JE002698.
- McSween, H.Y., Wyatt, M.B., Gellert, R., Bell, J.F., Morris, R.V., Herkenhoff, K.E., Crumpler, L.S., Milam, K.A., Stockstill, K.R., Tornabene, L.L., Arvidson, R.E., Bartlett, P., Blaney, D., Cabrol, N.A., Christensen, P.R., Clark, B.C., Crisp, J.A., Des Marais, D.J., Economou, T., Farmer, J.D., Farr, W., Ghosh, A., Golombek, M., Gorevan, S., Greeley, R., Hamilton, V.E., Johnson, J.R., Jolliff, B.L., Klingelhoefer, G., Knudson, A.T., McLennan, S., Ming, D., Moersch, J.E., Rieder, R., Ruff, S.W., Schroder, C., de Souza, P.A., Squyres, S.W., Wanke, H., Wang, A., Yen, A., Zipfel, J., 2006b. Characterization petrologic interpretation of olivine-rich basalts at Gusev Crater, Mars. *J. Geophys. Res.* 111 (E2), E02S10. doi:10.1029/2005JE002477.
- Mellon, M.T., Jakosky, B.M., Kieffer, H.H., Christensen, P.R., 2000. High-Resolution thermal inertia mapping from the Mars Global Surveyor Thermal Emission Spectrometer. *Icarus* 148, 437–455.
- Michael, G., Neukum, G., 2008. Surface dating: software tool for analysing crater size-frequency distributions including those showing partial resurfacing events. Lunar and Planetary Science Conference, p. 39. abstract 1780.
- Michael, G., Neukum, G., 2010. Planetary surface dating from crater size-frequency distribution measurements: partial resurfacing events and statistical age uncertainty. *Earth Planet. Sci. Lett.* 294, 223–229 (this issue).
- Milam, K.A., Stockstill, K.R., Moersch, J.E., McSween, H.Y., Tornabene, L.L., Ghosh, A., Wyatt, M.B., Christensen, P.R., 2003. THEMIS characterization of the MER Gusev Crater landing site. *J. Geophys. Res.* 108 (E12), 8078.
- Morris, R.V., Klingelhoefer, G., Schroder, C., Rodionov, D.S., Yen, A., Ming, D.W., de Souza, P.A., Fleischer, I., Wdowiak, T., Gellert, R., Bernhardt, B., Evlanov, E.N., Zubkov, B., Foh, J., Bonnes, U., Kankleit, E., Gutlich, P., Renz, F., Squyres, S.W., Arvidson, R.E., 2006. Mossbauer mineralogy of rock, soil, dust at Gusev crater, Mars: Spirit's journey through weakly altered olivine basalt on the plains pervasively altered basalt in the Columbia Hills. *J. Geophys. Res.* 111 (E2), E02S13. doi:10.1029/2005JE002584.
- Neukum, G., 1983. Meteoritenbombardement und Datierung planetarer Oberflächen. Habilitation Dissertation for Faculty Membership, University of Munich, 186.
- Neukum, G., Wise, D.U., 1976. Mars – standard crater curve and possible new time scale. *Science* 194, 1381–1387.
- Neukum, G., Ivanov, B.A., Hartmann, W.K., 2001. Cratering records in the inner solar system in relation to the lunar reference system. *Space Sci. Rev.* 96, 55–86.
- Neukum, G., Basilevsky, A.T., Kneissl, T., Chapman, M.G., van Gasselt, S., Michael, G., Jaumann, R., Hoffmann, H., Lanz, J., 2010. The geologic evolution of Mars: episodicity of resurfacing events and ages from cratering analysis of image data and correlation with radiometric ages of Martian meteorites. *Earth Planet. Sci. Lett.* 294, 204–222 (this issue).
- Nyquist, L.E., Bogard, D.D., Shih, C.-Y., Greshake, A., Stöfler, D., Eugster, O., 2001. Ages and geologic histories of Martian meteorites. In: Kallenback, R., Geiss, J., Hartmann, W. (Eds.), *Chronology and Evolution of Mars*. ISSI Space Science Series #96. Kluwer, Amsterdam, pp. 105–164.
- Powell, D., 1992. Interpretation of Geological Structures through Maps: An Introductory Practical Manual. Longman, 192 pp.
- Rice, J.W., 2005. The origin of the Columbia Hills, *Eos Trans. AGU, Fall Meet. Suppl.* 86 (52) Abstract P21A-0133.
- Robinson, M.S., Mouginsmark, P.J., Zimbelman, J.R., Wu, S.S.C., Ablin, K.K., Howingtonkraus, A.E., 1993. Chronology, eruption duration, atmospheric contribution of the Martian volcano Apollinaris-Patera. *Icarus* 104, 301–323.
- Schneeberger, 1989. Episodic channel activity at Ma'adim Vallis, Mars. Lunar Planetary Science Conference, p. 20. Abstract 964.
- Scott, E.R.D., Tanaka, K.L., 1986. Geologic map of the western equatorial region of Mars, scale 1:15 000 000, U.S. Geological Survey Misc. Geol. Invest. Map, I-1802-A.
- Scott, D.H., Morris, E.C., West, M.N., 1978. Geologic map of the Aeolis quadrangle of Mars. U.S. Geological Survey Miscellaneous Investigation Series p. Map I-1111 scale 1:5M.
- Sharp, R.P., 1973. Mars – fretted chaotic terrains. *J. Geophys. Res.* 78, 4073–4083.
- Sharp, R.P., Malin, M.C., 1975. Channels on Mars. *Geol. Soc. Amer. Bull.* 86, 593–609.
- Solomon, S.C., Aharonson, O., Aurnou, J.M., Banerdt, W.B., Carr, M.H., Dombard, A.J., Frey, H.V., Golombek, M.P., Hauck II, S.A., Head III, J.W., Jakosky, B.M., Johnson, C.L., McGovern, P.J., Neumann, G.A., Phillips, R.J., Smith, D.E., Zuber, M.T., 2005. New perspectives on ancient Mars. *Science* 307, 1214–1220.
- Squyres, S.W., Arvidson, R.E., Bell, J.F., Bruckner, J., Cabrol, N.A., Calvin, W., Carr, M.H., Christensen, P.R., Clark, B.C., Crumpler, L., Des Marais, D.J., d'Uston, C., Economou, T., Farmer, J., Farrand, W., Folker, W., Golombek, M., Gorevan, S., Grant, J.A., Greeley, R., Grotzinger, J., Haskin, L., Herkenhoff, K.E., Hviid, S., Johnson, J., Klingelhoefer, G., Knoll, A., Landis, G., Lemmon, M., Li, R., Madsen, M.B., Malin, M.C., McLennan, S.M., McSween, H.Y., Ming, D.W., Moersch, J., Morris, R.V., Parker, T., Rice, J.W., Rieder, L., Rieder, R., Sims, M., Smith, M., Smith, P., Soderblom, L.A., Sullivan, R., Wanke, H., Wdowiak, T., Wolff, M., Yen, A., 2004. The Spirit Rover's Athena Science Investigation at Gusev Crater, Mars. *Science* 305, P794.
- Squyres, S.W., Arvidson, R.E., Blaney, D.L., Clark, B.C., Crumpler, L., Farr, W.H., Gorevan, S., Herkenhoff, K.E., Hurowitz, J., Kusack, A., McSween, H.Y., Ming, D.W., Morris, R.V., Ruff, S.W., Wang, A., Yen, A., 2006. Rocks of the Columbia Hills. *J. Geophys. Res.* 111 (E2), E02S11. doi:10.1029/2005JE002562.
- Stewart, E.M., Head, J.W., 2001. Ancient Martian volcanoes in the Aeolis region: new evidence from MOLA data. *J. Geophys. Res.* 106 (E8), 17505–17513.
- Wang, A., Haskin, L.A., Squyres, S.W., Jolliff, B.L., Crumpler, L., Gellert, R., Schroder, C., Herkenhoff, K., Hurowitz, J., Tosca, N.J., Farr, W.H., Erson, R., Knudson, A.T., 2006a. Sulfate deposition in subsurface regolith in Gusev crater, Mars. *J. Geophys. Res.* 111 (E2), E02S17. doi:10.1029/2005JE002513.
- Wang, A., Korotev, R.L., Jolliff, B.L., Haskin, L.A., Crumpler, L., Farr, W.H., Herkenhoff, K.E., de Souza, P., Kusack, A.G., Hurowitz, J.A., Tosca, N.J., 2006b. Evidence of phyllosilicates in Woolly Patch, an altered rock encountered at West Spur, Columbia Hills, by the Spirit rover in Gusev crater, Mars. *J. Geophys. Res.* 111 (E2), E02S16. doi:10.1029/2005JE002516.
- Werner, S.C., Ivanov, A.B., Neukum, G., van Kan, M., Zegers, T.E., Foing, B.H., Greeley, R., Williams, D.A., 2005. Evolutionary history of Gusev – the MER landing site – seen by MEX-HRSC. Lunar Planetary Science Conference, p. 36. Abstract 1777.